Pergamon

Progress in Oceanography •• (2001) ••–••

Progress in Oceanography

www.elsevier.com/locate/pocean

Winter-to-winter recurrence of sea surface temperature, salinity and mixed layer depth anomalies

Michael A. Alexander *, Michael S. Timlin, James D. Scott

NOAA-CIRES, Climate Diagnostics Center, Boulder, Colorado, USA

Abstract

The mean seasonal cycle of mixed layer depth (MLD) in the extratropical oceans has the potential to influence temperature, salinity and mixed layer depth anomalies from one winter to the next. Temperature and salinity anomalies that form at the surface and spread throughout the deep winter mixed layer are sequestered beneath the mixed layer when it shoals in spring, and are then re-entrained into the surface layer in the subsequent fall and winter. Here we document this 're-emergence mechanism' in the North Pacific Ocean using observed SSTs, subsurface temperature fields from a data assimilation system, coupled with atmosphere-ocean model simulations. Observations indicate that the dominant large-scale SST anomaly pattern that forms in the North Pacific during winter recurs in the following winter. The model simulation with mixed layer ocean physics reproduced the winter-to-winter recurrence, while model simulations with observed SSTs specified in the tropical Pacific and a 50 m slab in the North Pacific did not. This difference between the model results indicate that the winter-to-winter SST correlations are the result of the re-emergence mechanism, and not of similar atmospheric forcing of the ocean in consecutive winters. They also indicate that SST anomalies in the tropical Pacific associated with El Niño are not essential for re-emergence to occur.

The recurrence of observed SST and simulated SST and SSS anomalies are found in several regions in the central North Pacific, and are quite strong in the northern (>50°N) part of the basin. The winter-to-winter autocorrelation of SSS anomalies exceed those of SST, since only the latter are strongly damped by surface fluxes. The re-emergence mechanism also has a modest influence on MLD through changes in the vertical stratification in the seasonal thermocline. © 2001 Published by Elsevier Science Ltd.

Contents

* Corresponding author. Address: R/CDC1, 325 Broadway, Boulder, CO 80303-3328.
E-mail address: maa@cdc.noaa.gov (M.A. Alexander).

0079-6611/01/$ - see front matter © 2001 Published by Elsevier Science Ltd.
PII: S0079-6611(01)00015-5

1. Introduction

El Niño and the Southern Oscillation (ENSO) is a coupled atmosphere-ocean phenomenon in the equatorial Pacific that varies over a period of about 2–7 years, and has a significant impact on climate variability and ecosystems over the globe. During strong El Niño events, drastic changes occur in the eastern tropical Pacific Ocean: rainfall is greatly enhanced, sea surface temperatures (SSTs) warm by more than 3°C, the normal coastal upwelling of cold nutrient rich water ceases and populations of many marine species decline precipitously (Barber & Chavez, 1983; Philander, 1990; Glynn, 1990). ENSO also influences conditions in the North Pacific; coastal Kelvin waves act to warm the water within a ~100 km of the North American coast (Enfield & Allen, 1980; Pares-Sierra & O'Brien, 1989; Meyers, Johnson, Liu, O'Brien, & Spiesberger, 1996), while changes in the atmospheric circulation cools the central Pacific Ocean and warms the eastern third of the basin via changes in air-sea heat fluxes (Alexander, 1992; Lau & Nath, 1996). ENSO induced changes in currents, temperatures, and other environmental factors over the North Pacific influences fish populations, for example by changing the migration routes of salmon and tuna (Mysak, 1986) and the abundance of rockfish (Yoklavich, Loeb, Nishimoto, & Daly, 1996).

There are several other processes that also affect climate variability in the North Pacific on time scales that are both longer and shorter in duration than ENSO. A number observational studies have documented decadal (>~7 years) variability in the North Pacific (Tanimoto, Iwasaka, Hanawa, & Toba, 1993; Trenberth & Hurrell, 1994; Mantua, Hare, Zhang, Wallace, & Francis, 1997; Nakamura, Lin, & Yamagata, 1997). Several studies have proposed that, like ENSO, conditions in the tropical Pacific govern some of this low frequency variability (Graham, Barnett, Wilde, Ponater, & Schubert, 1994; Trenberth & Hurrell, 1994). But others have implicated air-sea interaction and ocean dynamics at mid-latitudes as another key source of this variability (Latif & Barnett, 1994, 1996; Jin, 1997; Talley, 1999).

Widespread ecological fluctuations on decadal time scales have been recorded. Many studies have focused on ecosystem changes associated with an abrupt cooling in the central North Pacific that began in 1976 and lasted until 1988. Venrick, McGowan, Cayan, and Hayward (1987) found that chlorophyll concentrations in the water column, an indicator of primary productivity, increased during this period, while Brodeur and Ware (1992) and Roemmich and McGowan (1995) noted changes in zooplankton abundance. Ebbesmeyer et al. (1991) documented an abrupt

transition in many land and marine species around 1976, and several studies, including McFarlane and Beamish (1992) and Polovina et al. (1994) have found evidence of fish stocks changing around this time. Taken together these studies suggest that the climate fluctuations changes the growth and composition of phytoplankton, which in turn affect the higher trophic levels. Results from Beamish and Boullion (1993), Francis and Hare (1994) and Mantua et al. (1997) indicate that the regime change observed in the 1970s was not a unique climatic event, but one of a sequence of interdecadal climate fluctuations that occurred during the 20th century.

On annual and shorter time scales variability in the large-scale patterns of extratropical SST anomalies has mainly been attributed to local processes, including air-sea heat fluxes and vertical mixing in the upper ocean (Gill & Niiler, 1973; Frankignoul & Reynolds, 1983; Frankignoul, 1985; Delworth, 1996). The surface layer of most of the world's oceans is vertically well-mixed with nearly uniform temperature and salinity. In response to the seasonal cycle in wind stirring and surface buoyancy forcing, the ocean mixed layer deepens through fall and winter as a result of entrainment and then reforms close to the surface in spring and remains shallow through late summer. In the North Pacific the mean mixed layer depth (MLD) ranges from ~20 m in summer to >100 m in winter (Fig. 1), any departures of MLD from the seasonal average can significantly influence SSTs (Elsberry & Garwood, 1978; Alexander, Scott, & Deser, 2000).

Mixed layer depth is a critical factor in phytoplankton production, since entrainment of deeper water into the mixed layer not only increases the supply of nutrients to the euphotic zone, but also mixes phytoplankton deeper to where there is less light (or even insufficient light) available for photosynthesis (Cullen & Lewis, 1988; Mann & Lazier, 1991; Denman & Gargett, 1995). Several studies, including Marra and Ho (1993), Sarmiento et al. (1993), Fasham (1995) and Doney, Glover, and Najjar (1996) have examined the relationship between upper ocean mixing

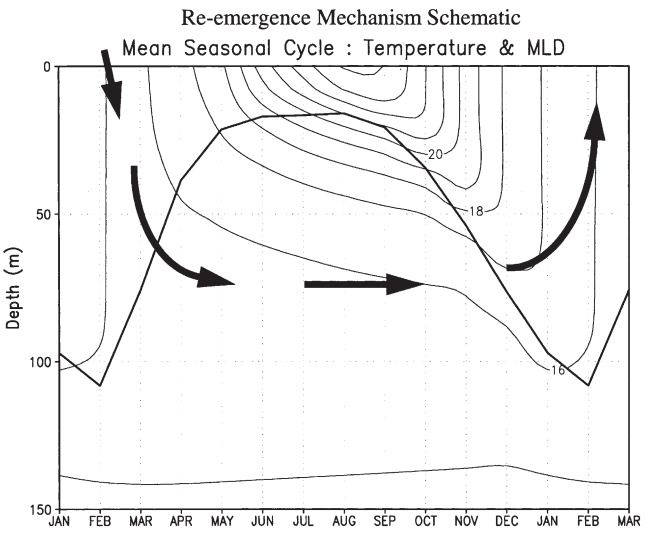

Fig. 1. Mean seasonal cycle of upper ocean temperature (°C) and mixed layer depth (m) for the central North Pacific (28°–42°N, 164°W–148°W) from the AGCM–MLM simulation. The arrows indicate the path of the re-emergence mechanism where anomalies created in winter are stored in the summer seasonal thermocline and are re-entrained into mixed layer when it deepens in the following fall and winter.

and biological productivity over the course of the seasonal cycle using coupled biological-physical models. Polovina, Mitchum, and Evans (1995) found that atmospheric forcing over the North Pacific lead to decadal variations in MLD, which in turn, strongly influenced biological productivity.

The seasonal cycle of MLD has the potential to influence conditions in the upper ocean from one winter to the next. Namias and Born (1970, 1974) were the first to note a tendency for mid-latitudinal SST anomalies to recur from one winter to the next without persisting through the intervening summer. They speculated that temperature anomalies form at the surface, spread throughout the deep winter mixed layer, and then persist beneath the mixed layer when it shoals in spring. The thermal anomalies are then incorporated into the stable summer seasonal thermocline (30–100 m) where they are insulated from surface fluxes that generally act to damp the original SST anomalies. When the mixed layer deepens again in the following fall, the anomalies become re-entrained into the surface layer and so again influence SST. Using subsurface temperature data from ocean weather ships and one-dimensional mixed layer model simulations Alexander and Deser (1995) have found that this 're-emergence mechanism' (shown schematically in Fig. 1) occurs at several locations away from strong ocean currents. Bhatt, Alexander, Battisti, Houghton, and Keller (1998) and Watanabe and Kimoto (2000) found further evidence for the re-emergence of SST anomalies in the North Atlantic Ocean. Alexander, Deser, and Timlin (1999) used several ocean temperature datasets to show that the re-emergence mechanism occurs across much of the North Pacific Ocean, where the dominant SST anomaly pattern that forms during late winter, reappear in the following fall/winter, although it has little persistence at the surface through the summer.

In this study, we expand on the work of Alexander et al. (1999) by addressing the following questions: Can we simulate the re-emergence process in the North Pacific using a coupled atmosphere-ocean model? The re-emergence mechanism has not been well documented north of 50°N in the Pacific Ocean; is it strong in this region where winter MLDs are relatively deep? Could SST anomalies reappear in the North Pacific from one winter to the next as a result of atmospheric forcing, such as consecutive winters of a stronger than normal Aleutian low, rather than by the re-emergence mechanism? Is ENSO critical for the winter-to-winter recurrence of SST anomalies over the North Pacific? Does re-emergence influence fields other than temperature that also have the potential to influence other environmental characteristics, such as salinity and mixed layer depth?

2. Observations and model simulations

In this study we have use SST observations, temperature analyses from an ocean data assimilation system, and coupled atmosphere-ocean model simulations to examine the re-emergence mechanism over the North Pacific. The gridded SST data, from Smith, Reynolds, Livezey, and Stokes (1996) used a statistical method to fill in data voids and to create fields that emphasize large-scale features. Global monthly SST fields are available from their analyses on a 2°×2° grid for 1950–1992. From 1993–2000 we use the SSTs on a 1°×1° grid based on the Reynolds and Smith (1994) optimal interpolation scheme.

Currently, there are insufficient raw upper ocean temperature measurements to document the

evolution of monthly temperature anomalies over the North Pacific. One method of obtaining the necessary spatial and temporal resolution is to use an assimilation system that combines ocean data with a dynamic ocean model that is forced by the observed atmospheric conditions. Here, we use monthly temperature fields obtained from the ocean data assimilation system at the National Center for Environmental Prediction (NCEP). The NCEP ocean assimilation system has been described by Derber and Rosati (1989) and Ji, Leetmaa, and Derber (1995). It consists of observed SST data taken from satellites and ships, plus subsurface thermal profiles obtained from expendable bathythermographs, all of which are blended with fields from an ocean general circulation model. The system domain is between 35°S and 45°N in the Pacific. The upper ocean is well resolved with 10 (15) levels in the upper 100 (200) m. We have assumed that the temperature obtained from the top level (5m) is representative of the SST. We use monthly mean temperatures from the assimilation system from January 1980 through to June 1998.

Most of the model results presented here are derived from a 50-year simulation of a global coupled atmosphere-ocean model. The model has been described in detail by Alexander et al. (2000), and consists of the Geophysical Fluid Dynamics Lab (GFDL) atmospheric general circulation model (AGCM) connected to an upper ocean mixed layer model (MLM). By using a coupled model we avoid the very difficult task of finding appropriate surface boundary conditions for the ocean model. The MLM is comprised of a grid of independent column models each of which is aligned with the AGCM grid and includes surface fluxes and the turbulent entrainment of water into the surface mixed layer, but not mean vertical motions or horizontal processes.

The MLM simulates SST (which is equivalent to the mixed layer temperature), sea surface salinity (SSS), and mixed layer depth (MLD). The SST tendency primarily depends on the net surface heat flux (Q_{net}), the heat flux through the base of the mixed layer resulting from entrainment (Q_{we}), and to a lesser degree on solar radiation that penetrates through the base of the mixed layer and molecular diffusion. The SSS tendency is regulated by precipitation minus evaporation, entrainment and molecular diffusion. Observed estimates of MLD are often based on the depth where temperature or density differs from the surface by a prescribed amount (e.g. Monterey & Levitus, 1997). However, here the MLD is computed directly by the MLM based on the turbulent kinetic energy equation following the formulation of Gaspar (1988). The mixed layer shoals by reforming closer to the surface, there is no entrainment at that time, and the MLD is the depth at which there is a balance between surface heating (positive buoyancy flux), wind stirring and dissipation. The MLD deepens via entrainment, which is primarily generated by wind stirring and surface cooling, but is impeded by the density step at the base of the mixed layer. The density step depends on the temperature and salinity within and just below the mixed layer. The region beneath the mixed layer is represented by a multi-layer system where heat is redistributed via convective overturning, vertical diffusion, and penetrating solar radiation.

By design, the AGCM-MLM simulation enables us to isolate the affects of midlatitude air-sea interaction and mixed layer physics, since it does not include currents or large-scale waves. Some AGCMs coupled to very coarse ocean GCMs or even slab ocean models display large SST variability in the tropical Pacific that bears some resemblance to ENSO (Meehl, 1990; Kitoh, Motoi, & Koide, 1999). However, this is not the case with in our AGCM-MLM experiment, where SST variability in the eastern equatorial Pacific is very small (see Figs. 3 and 4; Alexander et al., 2000).

We will also examine a second set of model experiments in which the GFDL AGCM has observed SSTs prescribed as boundary conditions in the tropical Pacific Ocean between approxi-

mately 25°N–25°S for the years 1950–1995. Outside of this domain the AGCM is coupled to a 50 m slab model over the remainder of the global ocean. There are four of these simulations that differ only in their initial atmospheric state. In keeping with previous naming conventions, these simulations are referred to as the 'tropical ocean global atmosphere'–50 m slab ocean (TOGA–50 m) experiment. Because of errors in the atmospheric fluxes and the absence of ocean heat transport, a surface heat flux correction is applied in both the TOGA–50 m and the AGCM-MLM experiments, in order to maintain a reasonable SST climatology.

The analyses have been performed using monthly anomalies, defined as the departure of the mean value for a given month from the long-term monthly mean. The fields from both model and observations used in the pattern analyses in section 3.b have been interpolated onto a 4°×4° grid.

3. Results

3.1. Regional analyses

The mean seasonal cycle of temperature and mixed layer depth from the 50-year AGCM-MLM simulation are shown for a region in the central North Pacific in Fig. 1. The MLD reaches a maximum of ~110 m in February and shoals rapidly in spring, reaching a minimum depth of ~20 m from May through September. A seasonal thermocline, where the temperature decreases rapidly with depth, forms in the summer between the base of the mixed layer and ~70 m. The seasonal cycle of temperature and mixed layer depth has the same basic structure over most of the North Pacific as shown in Fig. 1. The main differences between regions are: 1) the depth of the mixed layer in winter; 2) the annual mean temperature, and 3) the magnitude of the seasonal cycle, which is larger in the West Pacific than in the East Pacific. While the model simulates the key aspects of the seasonal cycle necessary for reproducing the re-emergence mechanism, there are some differences with observations (not shown), the simulated MLD is ~10% too shallow in fall and winter, and, as a result, the temperature maximum does not penetrate as deep in the MLM.

We examine the re-emergence mechanism in regions where previous analyses have suggested that it is strong, i.e. along the North American coast in the east Pacific, to north of Hawaii in the central Pacific, and along 40°N in the west Pacific. Regressions between SST anomalies in February–March–April (FMA) with temperature anomalies as a function of depth and month are shown in Fig. 2 for 'observations' from the NCEP data assimilation system and the MLM. The regression analyses provides a linear estimate of how a SST anomaly of 1°C in spring evolves from the previous January through the following April, and allows the magnitude of an anomaly to be tracked through the full re-emergence process. A 1°C anomaly is fairly large, as the standard deviation of SST is about $\frac{1}{2}$–$\frac{3}{4}$°C in late winter. The regressions indicate the re-emergence mechanism occurs in all three regions in both the model and the observations. High regression values that extend over the deep winter mixed layer, are maintained both in and below the seasonal thermocline, but they decay at the surface in summer, only to increase again at the surface in the following fall/winter.

Several factors influence the timing and strength of the re-emergence mechanism including geographic variation in the mean seasonal cycle of mixed layer depth. The maximum MLD in the North Pacific increases from about 80 m along the west coast of North America, to 120 m

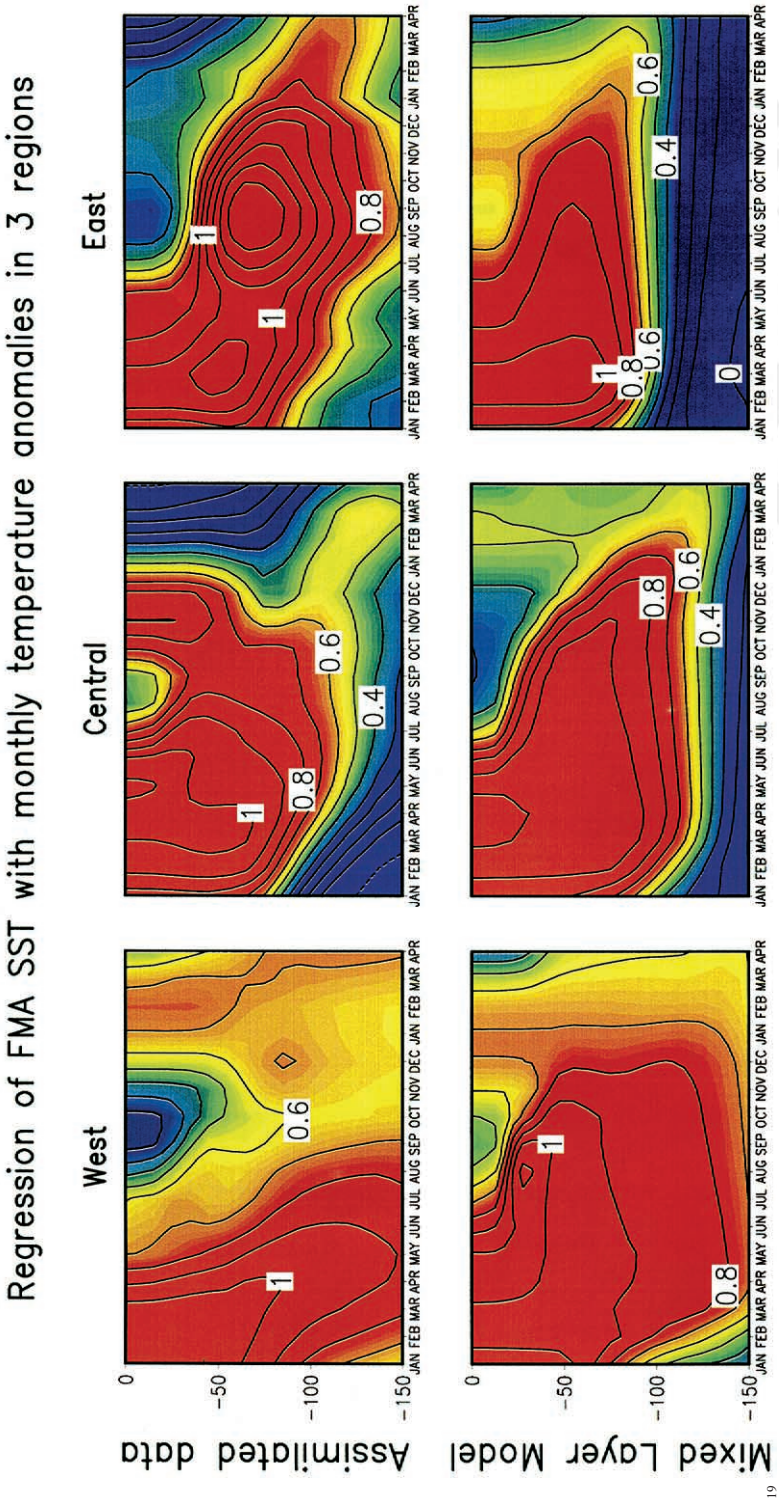

Fig. 2. Monthly SST anomalies from January through April of the following year regressed on SST anomalies averaged over the first February–March–April (FMA) period in the eastern (26N°–42°N, 132°W–116°W), central (26N°–42°N, 164°W–148°W), and western (38°N–42°N, 160°E–180°) Pacific. The central region is the same as in Fig. 1. Values are computed from observations provided by the NCEP ocean assimilation system for the years 1980–1998 (top) and from the 50-year AGCM–MLM simulation (bottom). The contour interval is 0.1°C per 1°C in FMA.

in the central Pacific, and to 200 m to the east of Japan (Bathen, 1972; Deser, Alexander, & Timlin, 1996; Alexander et al., 2000). As a result, the depth to which temperature anomalies penetrate in late winter increases from east to west, especially in the MLM as suggested by Fig. 2.

The regression values also suggest differences in the structure of the re-emergence mechanism between the data and the MLM, shown in the top and bottom panels of Fig. 2, respectively. In observations, the temperature anomalies created in winter continue to propagate down with time, as a result of subduction and complex turbulence processes. Whereas in the MLM, without these processes, temperature anomalies persist at nearly the same depth throughout summer and fall. In addition, in the West Pacific the temperature anomalies return to the surface later in the year in the data relative to the model, while the reverse happens in the central Pacific. In the eastern region, the observed regression values surprisingly increase with time from spring to summer, reaching a maximum of 1.3–1.4°C between 65–80 m in August–October for a 1°C in FMA; in the MLM the values decrease slightly during this time. In general, one would not expect anomalies to increase in magnitude as a result of the re-emergence mechanism unless it induces some additional changes in the upper ocean.

One possible explanation for the differences between observations and the model seen in Fig. 2 and for regression values >1.0 is uncertainty in the estimates resulting from the finite sample size, especially values from the data assimilation system where the record is only 18-years long. The 95% confidence interval about the observed regression value, computed following Snedecor and Cochran (1981), is on the order of ± 0.3°C in the east Pacific between 50–100 m in summer. Thus, most of the large regression values seen at depth in summer in this region are not significantly different than 1.0°C. An examination of the confidence intervals in the MLM and observations as a function of depth, time and region indicate that while the broad temperature anomaly patterns associated with re-emergence can be confirmed, the detailed structure of the patterns are not reliable. Real world processes may also contribute to the large temperature anomalies in the seasonal thermocline in the east Pacific, including variability in the California current system and coastally trapped waves induced by the re-emergence mechanism. Additional causes for model-data differences include errors in the temperatures obtained from the data assimilation system, and deficiencies in the AGCM–MLM.

The relatively deep winter mixed layers (>120 m) in both the model and observations north of 50°N in the Pacific suggest that the winter-to-winter persistence of SSTs could be strong there. Alexander and Deser (1995) found evidence for the re-emergence mechanism at weather ship P (50°N, 145°W). However, the NCEP ocean assimilation only extended to 45°N and most broad scale examinations of this process were performed farther to the south. Here we show correlations at 52°N between SST anomalies in FMA with monthly SST anomalies from the previous January through May of the following year. These autocorrelations are shown in Fig. 3 for both the Smith et al. (1996) 50-year SST data set and from the 50-year MLM simulation in each grid square between 160°E and 130°W. Across the basin in both observations and the model, high correlations in winter (>0.7) decrease through spring reaching a minimum in summer (0.1–0.4) and then increase through fall and reach a maximum (>0.5) in the following winter. While the observed and simulated values are not identical, both indicate that the summer minima persist longer and are stronger in the eastern and western portions of the basin relative to the central Pacific, also the return to higher correlations occurs earlier in the central (160°W) than in the western (165°E) Pacific. With 50 samples the 95% confidence interval about a correlation of 0.5 is approximately

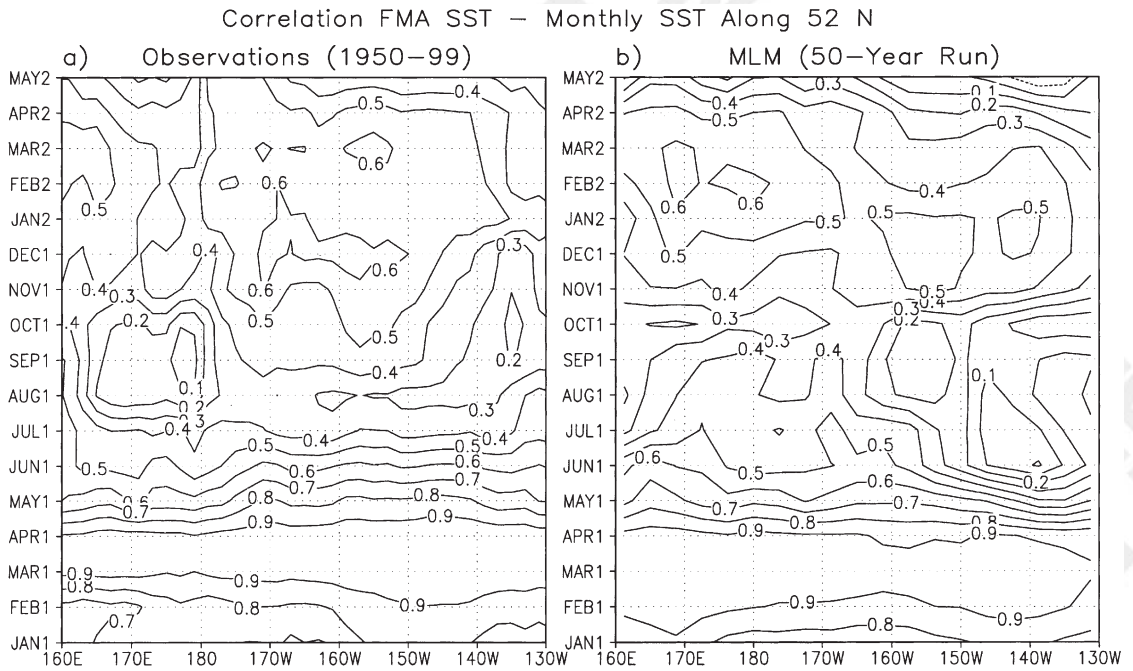

Fig. 3. Lead-lag correlations between SST anomalies in FMA and monthly SST anomalies from the previous January through May of the following year for each grid box along 52°N computed from a) observations from Smith et al. data set for the years 1950–99 and b) from the MLM.

±0.2 (Snedecor & Cochran, 1981). Thus, the correlations in spring, summer and the following fall-winter differ significantly from each other, but most of the differences between longitudes and between model and observations are not.

In the MLM, the net surface heat flux (Q_{net}) and the entrainment heat flux through the base of the mixed layer (Q_{we}) are the dominant terms that govern the SST tendency. Monthly anomalies of Q_{net} and Q_{we} regressed on the SST anomalies in FMA in the MLM are shown in Fig. 4. Since the fluxes often lead the SST anomalies the results are presented for a 20-month period from the previous October through the following May. The SST–Q_{net} regressions are maximum (>80 $Wm^{-2}°C^{-1}$) indicating that the surface flux anomalies into the ocean during winter are acting to create the initial SST anomalies in FMA. The primarily negative SST–Q_{net} regressions from May onward show that the surface fluxes act to damp the SST anomalies once they have been created. The large negative values centered at 155°W in the second February lead to the reversal in sign of the MLM SST anomalies from the winter to spring of year 2 as seen in Fig. 3b.

SST–Q_{we} regressions values (Fig. 4b) on the order of -25 $Wm^{-2}°C^{-1}$ in FMA indicate that entrainment tends to oppose Q_{net} and the initial development of the SST anomalies. This is partly because of the dilution of SST anomalies by the entrainment of water with thermal anomalies that are unrelated to those currently in the surface layer (see Frankignoul, 1985 for a more detailed discussion). The positive values of 20–25 $Wm^{-2}°C^{-1}$ indicate that the thermal anomalies created in FMA are returned to the surface mixed layer via entrainment in the following fall in the eastern Pacific and the following winter in the western Pacific. The timing of the surface and entrainment

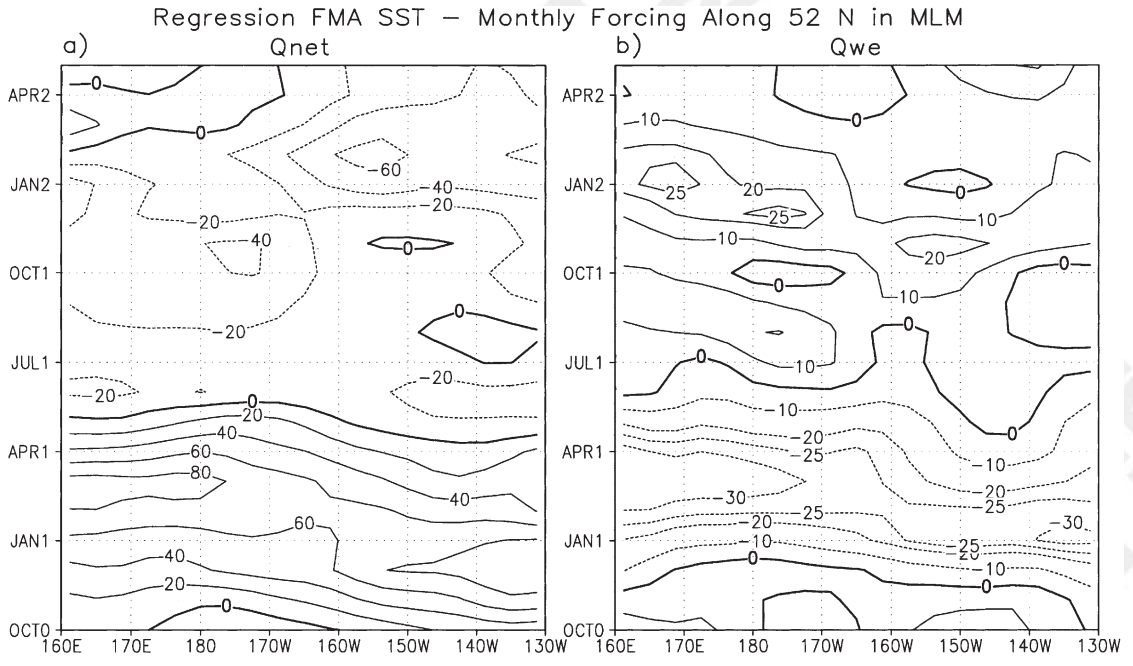

Fig. 4. a) Monthly surface heat flux (Q_{net}) and b) entrainment heat flux (Q_{we}) anomalies from January through May of the following year regressed on SST anomalies in the first FMA for each grid box along 52°N. Contour interval is 10 Wm^{-2} per °C, the zero contour is thickened, and the ±25 contour interval is shown for Q_{we}. The fluxes are obtained from the MLM and have been smoothed with a 9-point spatial smoother prior to calculating the regressions.

heat flux anomalies are consistent with the development of the SST anomalies in the MLM on monthly time scales: the Q_{net} and Q_{we} anomalies (Fig. 4) are concurrent with, or lead, the SSTs (Fig. 3b) and both occur 2–3 months earlier in the east, compared with the west Pacific.

In general the Q_{net} regression values exceed those of Q_{we}, suggesting that the net heat flux is the dominant term in generating SST anomalies. However, entrainment is important in the surface heat budget during fall and early winter. In addition, entrainment tends to be a very localized and episodic process and thus will be underestimated by a linear regression analyses based on monthly values. The re-emergence mechanism is primarily associated with just one component of the anomalous Q_{we}: the mean entrainment rate times the anomalous temperature jump at the base of the mixed layer (Alexander & Penland, 1996). The regression values between FMA SST and this component of Q_{we} have a similar evolution to those shown in Fig. 4b but are 20–40% greater in magnitude (not shown).

3.2. Basin-wide analyses

The behavior of thermal anomalies across the North Pacific over the seasonal cycle is examined using extended empirical orthogonal function analysis (EEOF). EOF analysis is a method for finding patterns in a field of variables. EEOF, as the name suggests isan extension of conventional EOF analyses, and indicates how the patterns evolve with time. This analysis has been used in several studies to examine the evolution of climate anomalies (e.g. Weare & Nasstrom, 1982;

Miller, Cayan, & White, 1998). Here, the leading EEOF of monthly SST anomalies from January through the following April (lags of 0–15 months) is computed from the covariance matrix, where the variance at each point in a month has been normalized by the average standard deviation of SST at all points in the domain during that month.

The evolution of the leading pattern of SST variability is presented in Fig. 5 as correlations between the first principal component, the time series that gives the sign and amplitude of EEOF 1, with the time series of monthly SST anomalies at individual grid points. The correlation maps are shown for every other month from January through April of the following year for: a) SST observations for 1950–1999; b) the AGCM–MLM simulation; and c) the set of four TOGA–50 m simulations.

Recall that the same AGCM is used in both types of simulations, but in the TOGA–50 m integrations SSTs are specified according to observations over the period 1950–1995 in the tropical Pacific, while SSTs are simulated by a 50 m slab model elsewhere over the global ocean. Thus, the TOGA–50 m experiments do have the ENSO signal in the tropical Pacific but do not have mixed layer physics in the North Pacific. EEOF 1 explains approximately the same amount of total variance (15%–18%) in observations and the two model simulations. The leading pattern of variability in the three analyses are also similar: all show anomalies of one sign from about 25°N–45°N in the central and west Pacific ringed by anomalies of the opposite sign. In observations and the MLM the magnitude of the pattern and the percentage of the total variance explained by EEOF1 (Fig. 6) decreases from March to a minumum in September; it then increases again, reaching a maximum in the following winter. However, in the TOGA–50 m simulations the magnitude decreases with time and the pattern nearly disappears by November. The ability of the AGCM–MLM, but not the TOGA–50 m, to simulate the evolution of the dominant pattern of SST variability over the North Pacific has several important implications: a) The winter-to-winter recurrence of SST anomalies is not the result of similar atmospheric forcing patterns from one winter to the next; b) ENSO events are not crucial for getting the winter-to-winter basin-wide SST anomaly pattern; and c) The MLM, with a variable MLD and the storage of thermal anomalies beneath the mixed layer, has the essential physics for reproducing the re-emergence mechanism.

While the leading pattern of variability is similar in the three panels of Fig. 5, the positive anomaly center in the central Pacific has a southwest to northeast tilt in the AGCM–MLM simulation, but has a nearly zonal orientation in observations and the TOGA–ML simulation. A likely explanation for this difference is the influence of ENSO on North Pacific SST anomalies via the 'atmospheric bridge' (Alexander, 1992; Lau & Nath, 1996) in observations and the TOGA–50 m simulations. The SST anomaly in the central North Pacific associated with ENSO is largest at around 35°N, 160°W and extends westwards towards central Japan, and thus projects strongly on the leading pattern of SST variability. Alexander et al. (1999) showed that the dominant pattern of temperature anomalies at depth in summer is correlated with SST anomalies in the tropical Pacific. Thus, while ENSO is not essential for the re-emergence mechanism to occur, it does influence the pattern of the SST anomalies that participate in the re-emergence process over the North Pacific.

Figs. 5 and 6 indicate that the decline in the leading pattern of variability in summer, especially in the west Pacific from 35°N–45°N is more pronounced in the MLM compared with observations. Zhang, Norris, and Wallace (1998) have suggested that the observed SST anomalies in the North

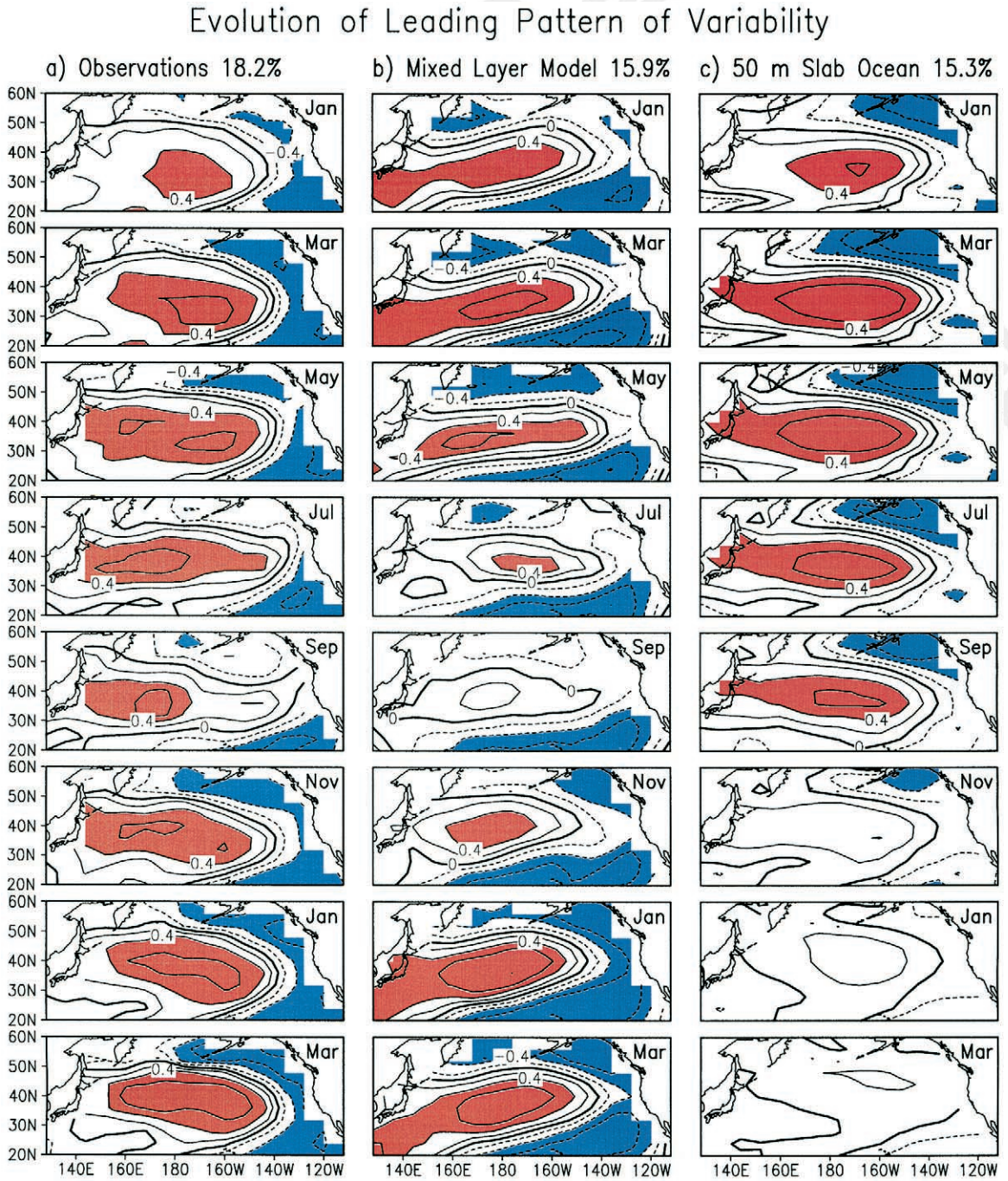
Evolution of Leading Pattern of Variability
a) Observations 18.2%
b) Mixed Layer Model 15.9%
c) 50 m Slab Ocean 15.3%
Jan
Mar
May
Jul
Sep
Nov
Jan
Mar
60N
50N
40N
30N
20N
140E 160E 180 160W 140W 120W

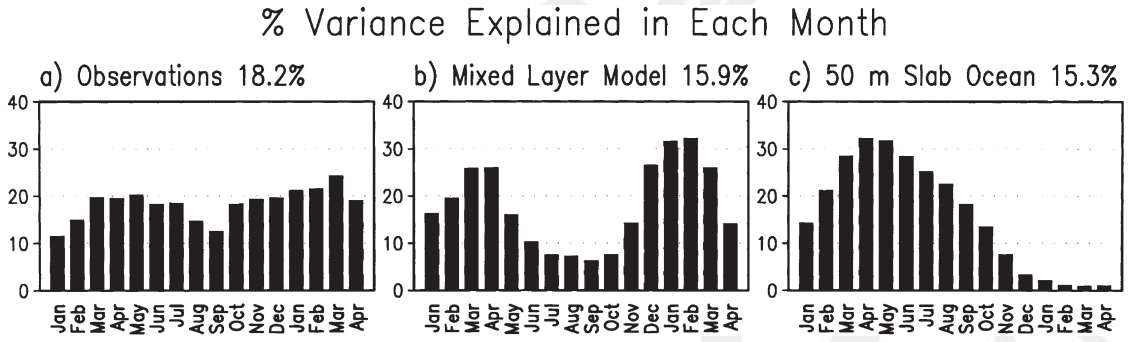

Fig. 6. The percentage variance of the monthly SST anomaly field over the North Pacific domain explained by EEOF 1 for a) the Smith dataset, b) the AGCM–MLM simulation and c) the 4 TOGA–50 m simulations. Results are presented for each month from January through April of the following year.

Pacific can persist from winter to summer and vice versa, although they attributed this persistence to positive feedbacks between stratiform clouds and ocean temperatures. Most AGCMs, including the one used here, do a poor job in simulating stratus clouds, and this leads to errors in SST anomalies in coupled models. Other processes not included in the AGCM–MLM that may also contribute to the maintenance of observed SST anomalies in the west Pacific through summer, included interannual and longer fluctuations in the heat transported by the Kuroshio extension and teleconnections with ENSO which appear to influence SSTs in the vicinity of 40°N, 160°E in July–September (Harrison & Larkin, 1998).

We now explore how the leading pattern evolves over time and depth by calculating EEOF 1 using monthly ocean temperature anomalies at 5 levels: (5, 27.5, 47.5, 65 and 85 m) from the AGCM–MLM simulation in the covariance matrix. The surface evolution of the dominant pattern (not shown) is nearly identical to the one shown for just SST in Fig. 5b. A contour plot of the percentage variance explained by EEOF 1 in each month from January through April of the following year as a function of depth is shown in Fig. 7. The leading EEOF explains ~23% of the total variance and more than 20% percent of the monthly variance from 0–85 m in the first winter, below 45 m in summer, and from 0–85 m in the following December–March. The leading pattern nearly disappears at the surface in summer, since it encompasses only 4% of the variance in September.

3.3. Impact of re-emergence on SSS and MLD

The limited number of salinity measurements and estimates of mixed layer depth make it impractical to study how anomalies in these fields evolve over the seasonal cycle from obser-

Fig. 5. The evolution of the leading pattern of SST variability over 20°N–60°N in the Pacific as indicated by EEOF 1 of monthly SST anomalies from January through April of the following year. The results are presented as the correlation between the principal component (time series) of EEOF 1 with the SST anomalies at the individual grid points for every other month beginning in January (the other months which are not shown indicate a similar evolution). Results are presented for a) the Smith dataset for the years 1950–1999, b) the AGCM–MLM simulation and c) the 4 TOGA–50 m simulations. For the latter, EEOF 1 was computed by appending the four 46-year runs to each other, creating an 184-year time series. The contour interval is 0.2 with values >0.4 shaded red and those <-0.4 shaded blue.

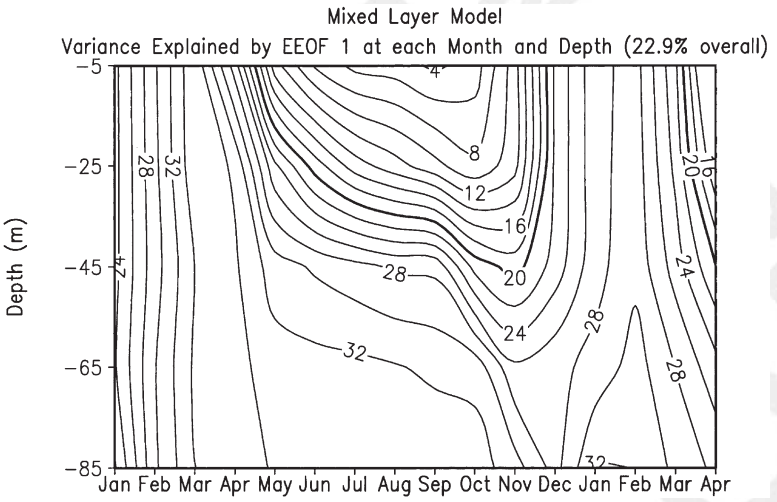

Fig. 7. The percentage variance of monthly temperature anomalies explained by EEOF 1 for the North Pacific domain (20°N–60°N) in the AGCM–MLM simulation when it is computed as a function of both time and depth. The five depth levels used are 5, 27.5, 47.5, 65 and 85 m. Results are presented for each month from January through April of the following year.

vations. Here we examine how the re-emergence mechanism influences sea surface salinity (SSS) and MLD in the AGCM–MLM simulation. The correlation between SSS anomalies in FMA and monthly SSS anomalies from the previous January through June of the following year for each grid square along 52°N is shown in Fig. 8a. Like the simulated SST anomalies, the SSS autocorrelations drop from high values in the first winter to a minimum in summer but rise to a second maximum in the following winter. However, except during summer to the west of 170°E, the SSS correlations tend to be 0.1–0.4 larger than those for SST after July. For example, the SSS and SST autocorrelation values in December at 160°W are 0.8 (Fig. 8a) and 0.5 (Fig. 3b), respectively. The higher correlations for SSS are consistent with the findings of Hall and Manabe (1997) who showed that SST anomalies are more highly damped by surface fluxes than SSS anomalies, since positive SST anomalies are followed by negative Qnet anomalies (Fig. 4a), i.e. warmer water will lose more heat to the atmosphere and vice versa. In contrast, SSS anomalies have a negligible impact on the net fresh water flux and so with little damping they would persist longer than SST anomalies.

The zonal average across the Pacific at 20°N, 30°N, 40°N and 50°N of autocorrelations based on SSS anomalies in FMA are shown in Fig. 8b. At 50°N and 40°N, the correlations drop to 0.4 in September and then increase to a maximum >0.7 in the following winter. The decrease of SSS correlation in summer is not as strong at 30°N, but the correlation values are similar to the two more northern latitudes during the following winter. At 20°N, the correlations decline to September and are then nearly constant through March. The differences in the autocorrelation functions with latitude is likely to be tied to the seasonal cycle of mixed layer depth, since the autocorrelation in precipitation-evaporation, which governs the surface fresh water flux, drops nearly to zero by June at all latitudes. At 20°N the mean seasonal cycle of MLD is relatively weak and the MLD is about twice as large in summer compared with the other latitudes, allowing

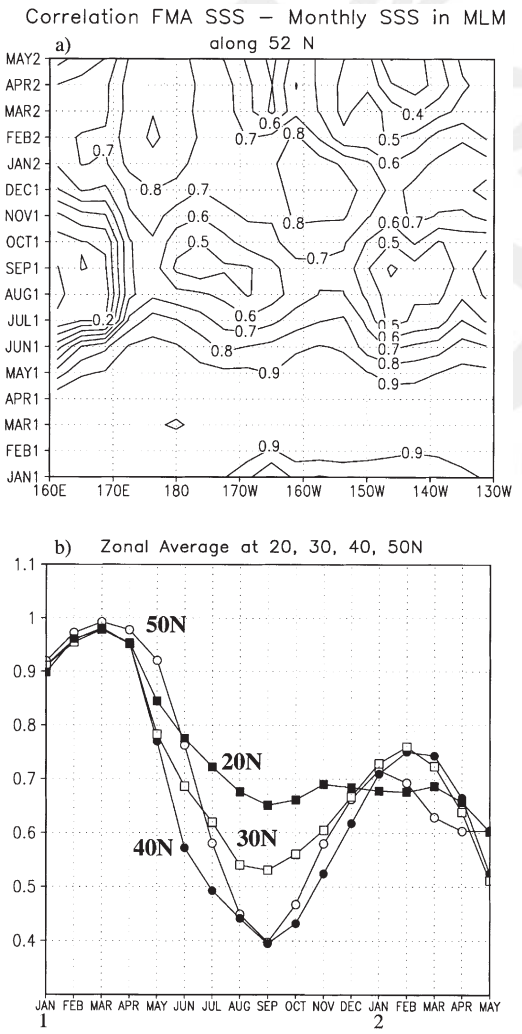

Fig. 8. Lead-lag correlations between SSS anomalies in FMA and monthly SSS anomalies from the previous January through June of the following year for a) grid boxes along 52°N and b) zonally averaged across the North Pacific along 20°N, 30°N, 40°N and 50°N from the AGCM–MLM simulation.

SSS anomalies to persist longer through summer but not to rebound as strongly in the following winter.

Correlations between SST anomalies in FMA and monthly MLD anomalies along 52°N in the MLM are shown in Fig. 9a. Since the MLD anomalies are much smaller and more variable than the SST or SSS anomalies they have been smoothed twice using a nine-point smoother in space prior to computing the correlations and then the correlation values have been smoothed with the same filter. The SST–MLD correlations are from January–May, near zero (−0.2 to 0.2) from June–September, and then positive from September–April across the entire basin. The maximum absolute value of the correlations is on the order of 0.4–0.45. The zonal average of the correlations between FMA SST anomalies and the monthly MLD anomalies at 20°, 30°, 40° and 50°N are

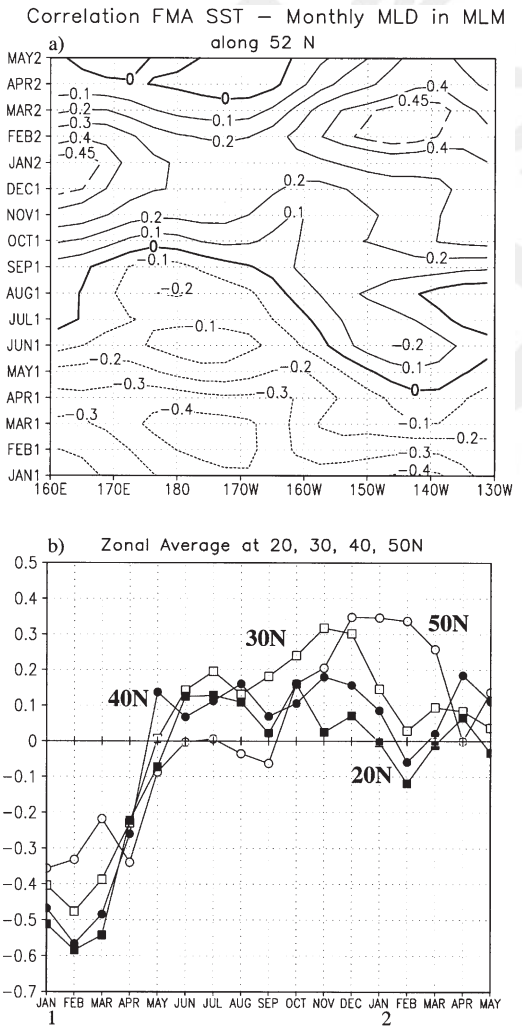

Fig. 9. Lead-lag correlations between SST anomalies in FMA and monthly MLD anomalies from the previous January through the following June for a) grid boxes along 52°N and b) zonally averaged across the North Pacific along 20°N, 30°N, 40°N and 50°N from the AGCM–MLM simulation. The contour interval is 0.1, the zero contour is thickened, and the 0.45 contour is shown with a dashed line.

presented in Fig. 9b. Because of the noise in the MLD anomaly fields, there is a fair amount of month-to-month variability in the SST–MLD correlations. Nevertheless, a trend is discernable at all latitudes with negative values in the first January–March that increase through spring and are generally positive though the following winter. The maximum correlations are modest with values of ~0.35 at 30°N and 50°N.

A negative concurrent relationship between SST and MLD has also been documented in the North Pacific by Polovina et al. (1995) and Deser et al. (1996). MLD and SST are anti-correlated since the atmospheric conditions, which lead to negative (colder) SST anomalies, enhanced surface cooling through stronger winds and colder drier air, also create positive (deeper) MLD anomalies

through convective plumes and mechanical mixing. The reverse is also true. Deser et al. (1996) show that the absolute value of negative concurrent SST–MLD correlations is greatest in winter, when the MLD is primarily controlled by mixing associated with surface the buoyancy forcing (Alexander et al., 2000).

The tendency towards positive correlations between winter SSTs and MLD anomalies in the following fall and winter is associated with the mean seasonal cycle of MLD and the re-emergence process. When the deep mixed layer in winter shoals, the water left behind affects the density profile in the seasonal pycnocline. If the winter mixed layer is warmer (and/or fresher) than normal then the vertical stratification will be weaker in the seasonal pycnocline when this anomaly is stored at depth in summer. As a result, the penetration depth of the mixed layer will increase for the same amount of surface forcing, especially during the main period of deepening in the following fall and winter. Thus, a positive SST anomaly in winter leads to a positive MLD anomaly in the following seasons, and vice versa. However, the modest positive correlation values in Fig. 9 and the results of Alexander et al. (2000) indicate that this is a secondary affect compared with the concurrent surface forcing of the mixed layer. We also note that in the MLM the MLD in one winter is not directly related that in the next since the autocorrelation of MLD anomalies decays rapidly and approaches zero by summer.

4. Summary and discussion

The winter-to-winter recurrence of SST anomalies in the North Pacific has been documented using observed SSTs, subsurface temperature fields from the NCEP's ocean data assimilation system and coupled atmosphere-ocean model simulations. Two types of model simulations have been analyzed; in one an AGCM is coupled to a predictive mixed layer ocean model (MLM), while in the second, the same AGCM is coupled to 50 m slab model outside the tropical region where observed SSTs are specified as boundary conditions. In the North Pacific, the former simulates a variable depth mixed layer and seasonal thermocline, while the latter includes the effects of ENSO but not the mixed layer processes. The observations and model simulations performed with the MLM show that temperature anomalies created in the deep winter mixed layer, are strongly damped in the shallow surface layer, but are stored in the seasonal thermocline in summer and returned to the surface via entrainment in the following winter. However, the model simulations with a 50 m slab ocean showed no evidence for re-emergence. The difference between the two indicates that the winter-to-winter recurrence of SST anomalies results from mixed layer physics and not from any similarity in atmospheric forcing in consecutive winters. In addition, while SST anomalies in the tropical Pacific associated with ENSO affect the wintertime SSTs in the North Pacific via changes in the extratropical atmospheric circulation, ENSO events are not essential for re-emergence to occur.

Extended EOF analyses indicates that the dominant large-scale SST anomaly pattern that forms in the North Pacific during winter, with anomalies of one sign in the central Pacific ringed by anomalies of the opposite sign, recurs in the following winter as a result of the re-emergence mechanism. While this pattern of SST anomalies is driven by the large-scale atmospheric forcing, the re-emergence process itself is primarily local in nature, since geostrophic advection and Rossby waves are relatively slow in the ocean and do not have sufficient time to change the

thermal patterns over the course of a year. However, some horizontal oceanic processes are able to shape the re-emergence signal. Anomalous heat transport associated with Ekman currents can create SST anomalies that subsequently undergo the re-emergence process. This is most pronounced in the western half of the Pacific along 40°N where the mean gradients of SST are strong. Near the ocean boundaries, temperature anomalies at depth in summer left behind by the retreating mixed layer may be transported by strong local currents and also have the potential to excite baroclinic coastally-trapped waves. However, it would be difficult to separate these affects from all the other process influencing temperatures in coastal environments.

Mid-latitude regions in the eastern, central, and western Pacific all show evidence of the re-emergence mechanism; differences between the three regions partly result from geographic variability in the mixed layer depth and the static stability of the upper ocean. The recurrence of both simulated and observed SST anomalies is quite strong in the sub-arctic region of North Pacific, where winter mixed layers are relatively deep. Alexander et al. (2000) found that the effective thermal capacity of the surface layer depends on the MLD in winter, thus in regions of deep mixed layers thermal anomalies are highly persistent from one winter to the next.

Ocean temperature anomalies that return to the surface in the fall and winter could influence the atmosphere, and in turn, changes in the atmosphere can alter SSTs. Thus, air-sea feedback has the potential to modify the SSTs associated with the re-emergence mechanism. One obvious mechanism whereby this occurs is through negative thermal feedbacks; i.e. upward heat fluxes are enhanced when the water is warmer and vice versa, which act to damp the SST anomalies. An open question is to what extent do the SSTs actually change the atmospheric circulation, which could have a non-negative and non-local impact on the ocean. Some studies suggest there is evidence for positive air-sea feedbacks (Peng, Mysak, Ritchie, Derome, & Douglas, 1995; Latif & Barnett, 1996) although this process is not universal and was not readily apparent in the AGCM–MLM simulations. Almost all studies have shown that the atmospheric response to mid-latitude SST anomalies is modest; thus the SST anomaly pattern associated with the return branch of the re-emergence mechanism is primarily controlled by the mixed layer physics.

In addition to ocean temperatures, the re-emergence mechanism also influences salinity and MLD. The autocorrelations of SSS anomalies exceed those of SST, since SST anomalies decay because of negative air-sea feedbacks, while SSS anomalies have a negligible affect on the surface freshwater flux. The re-emergence mechanism influences MLD in the following fall and winter through changes in the stratification in the seasonal thermocline. When the winter mixed layer shoals, anomalously cold (warm) water left behind will enhance (reduce) the density jump at the base of the mixed layer, and thus retard (enhance) the growth of the MLD in the following fall and winter. However, the re-emergence process has only a modest impact on MLD, since the latter is strongly influenced by other processes such as the concurrent surface buoyancy and wind stress forcing.

Through its impact on temperature, salinity and mixed layer depth, the re-emergence process may influence biological activity in the upper ocean. For example, changes in MLD in fall as a result of conditions in the previous winter, could alter the amount of time phytoplankton is able to reside in the euphotic zone. In addition, re-emergence could affect the primary productivity by changing the phytoplankton biomass and/or the amounts of nutrients available over the seasonal cycle. In some locations, such as western subtropical gyres, a spring bloom near the surface is followed by a relative maximum in phytoplankton within the seasonal thermocline (Doney et al.,

1996). Thus, conditions in late winter–early spring within the mixed layer have the potential to influence the amount of nutrients and/or phytoplankton in the seasonal thermocline, and thus the primary productivity at the surface in the subsequent fall and winter when the mixed layer deepens and re-entrains the water from below.

5. Uncited references

Deser & Blackmon, 1995; Kalnay et al., 1996; Lau & Chan, 1985; Norris, Zhang, & Wallace, 1998; Robertson, 1996; Weare, Navato, & Newell, 1976; White, 1995; Yukimoto et al., 1996; Zhang, Wallace, & Battisti, 1997

Acknowledgements

We thank Gabriel Lau and Isaac Held for providing to us the GFDL AGCM and model fields from the TOGA–50 m simulations. We also thank Clara Deser, Art Miller and an anonymous reviewer for their insightful comments on the manuscript. This research was supported by NOAA grant GC98-139.

References

Alexander, M. A. (1992). Midlatitude atmosphere-ocean interaction during El Niño. Part I: the North Pacific Ocean. *Journal of Climate*, *5*, 944–958.

Alexander, M. A., & Deser, C. (1995). A mechanism for the recurrence of wintertime midlatitude SST anomalies. *Journal of Physical Oceanography*, *25*, 122–137.

Alexander, M. A., Deser, C., & Timlin, M. S. (1999). The re-emergence of SST anomalies in the North Pacific Ocean. *Journal of Climate*, *12*, 2419–2433.

Alexander, M. A., & Penland, C. (1996). Variability in a mixed layer model of the upper ocean driven by stochastic atmospheric surface fluxes. *Journal of Climate*, *9*, 2424–2442.

Alexander, M. A., Scott, J. D., & Deser, C. (2000). Processes that influence sea surface temperature and mixed layer depth in a coupled model. *Journal of Geophysical Research*, *105*, 16823–16842.

Barber, R. T., & Chavez, F. P. (1983). Biological consequences of El Niño. *Science*, *222*, 1203–1210.

Bathen, K. H. (1972). On the seasonal changes in the depth of the mixed layer in the North Pacific Ocean. *Journal of Geophysical Research*, *77*, 7138–7150.

Beamish, R. J., & Boullion, D. R. (1993). Pacific salmon trends in relation to climate. *Canadian Journal of Fisheries and Aquatic Sciences*, *50*, 1002–1016.

Bhatt, U. S., Alexander, M. A., Battisti, D. S., Houghton, D. D., & Keller, L. M. (1998). Role of atmosphere-ocean interaction in North Atlantic climate variability. *Journal of Climate*, *11*, 1615–1632.

Brodeur, R. D., & Ware, D. M. (1992). Interannual and interdecadal changes in zooplankton biomass in the subarctic Pacific Ocean. *Fisheries Oceanography*, *1*, 32–38.

Cullen, J. J., & Lewis, M. R. (1988). The kinetics of algal photoadaptation in the context of vertical mixing. *Journal of Phytoplankton Research*, *10*, 1039–1063.

Delworth, T. (1996). North Atlantic interannual variability in a coupled ocean-atmosphere model. *Journal of Climate*, *9*, 2356–2375.

Denman, K. L., & Gargett, A. E. (1995). Biological-physical interactions in the upper ocean: the role of vertical and small scale mixing processes. *Annual Review of Fluid Mechanics*, *27*, 225–255.

Derber, J. D., & Rosati, A. (1989). A global oceanic data assimilation system. *Journal of Physical Oceanography*, *19*, 1333–1347.

Deser, C., Alexander, M. A., & Timlin, M. S. (1996). Upper ocean thermal variations in the North Pacific during 1970–1991. *Journal of Climate*, *9*, 1841–1855.

Deser, C., & Blackmon, M. L. (1995). On the relationship between tropical and north Pacific sea surface temperature variations. *Journal of Climate*, *8*, 1677–1680.

Doney, S. C., Glover, D. M., & Najjar, R. G. (1996). A new coupled one-dimensional biological-physical model for the upper ocean: applications to JGOFS Bermuda Atlantic time series study (BATS) sites. *Deep-Sea Research II*, *43*, 591–624.

Ebbesmeyer, C. C., Cayan, D. R., McClain, Nichols, F. H., Peterson, D. H., & Redmond, K. T. (1991). 1976 step in the Pacific climate: forty environmental changes between 1968–1975 and 1977–1984. In *Proceedings of the Seventh Annual Climate Workshop (PACLIM)* (pp. 115–126). Asilomar, CA, April, 1990.

Elsberry, R., & Garwood, R. W. (1978). Sea surface temperature anomaly generation in relation to atmospheric storms. *Bulletin of the American Meteorological Society*, *59*, 786–789.

Enfield, D. B., & Allen, J. S. (1980). On the structure and dynamics of monthly mean sea level anomalies along the Pacific coast of North and South America. *Journal of Physical Oceanography*, *10*, 557–588.

Fasham, M. J. R. (1995). Variations in the seasonal cycle in biological production in subartic oceans: a model sensitivity analysis. *Deep-Sea Research I*, *42*, 1111–1149.

Francis, R. C., & Hare, S. R. (1994). Decadal scale regime shifts in the large marine ecosystems of the North-east Pacific: a case for historical science. *Fisheries Oceanography*, *3*, 279–291.

Frankignoul, C. (1985). Sea surface temperature anomalies, planetary waves, and air-sea feedback in the middle latitudes. *Reviews of Geophysics*, *23*, 357–390.

Frankignoul, C., & Reynolds, R. W. (1983). Testing a dynamical model for mid-latitude sea surface temperature anomalies. *Journal of Physical Oceanography*, *13*, 1131–1145.

Gaspar, P. (1988). Modeling the seasonal cycle of the upper ocean. *Journal of Physical Oceanography*, *18*, 161–180.

Gill, A. E., & Niiler, P. P. (1973). The theory of the seasonal variability in the ocean. *Deep-Sea Research*, *20*, 141–177.

Glynn, P. (1990). *Global ecological consequences of the 1982–83 El Niño-Southern Oscillation.* Amsterdam: Elsevier 563 pp.

Graham, N. E., Barnett, T. P., Wilde, R., Ponater, M., & Scuhbert, S. (1994). On the roles of tropical and midlatitude SSTs in forcing annual to interdecadal variability in the winter Northern Hemisphere circulation. *Journal of Climate*, *7*, 1416–1442.

Hall, A., & Manabe, S. (1997). Can local linear stochastic theory explain sea surface temperature and salinity variability. *Climate Dynamics*, *13*, 167–180.

Harrison, D. E., & Larkin, N. K. (1998). El Niño-Southern Oscillation sea surface temperature and wind anomalies. *Reviews of Geophysics*, *36*, 353–399.

Ji, M., Leetmaa, A., & Derber, J. (1995). An ocean analyses system for seasonal to interannual climate studies. *Monthly Weather Review*, *123*, 460–480.

Jin, F. F. (1997). A theory for interdecadal climate variability of the North Pacific ocean-atmosphere system. *Journal of Climate*, *10*, 1821–1835.

Kalnay, E., Kanamitsu, M., Kistler, R., Collins, W., Deaven, D., & Gandin, L. et al. (1996). The NCEP/NCAR 40-year reanalysis project. *Bulletin of the American Meteorological Society*, *77*, 437–471.

Kitoh, A., Motoi, T., & Koide, H. (1999). SST variability and its mechanism in a coupled atmosphere-mixed layer ocean model. *Journal of Climate*, *12*, 1221–1239.

Latif, M., & Barnett, T. P. (1994). Causes of decadal climate variability over the North Pacific and North America. *Science*, *266*, 634–637.

Latif, M., & Barnett, T. P. (1996). Decadal climate variability over the North Pacific and North America: dynamics and predictability. *Journal of Climate*, *9*, 2407–2423.

Lau, K. M., & Chan, P. H. (1985). Aspects of the 40–50 day oscillation during the northern winter as inferred from outgoing longwave radiation. *Monthly Weather Review*, *113*, 1889–1909.

Lau, N.-C., & Nath, M. J. (1996). The role of the 'atmospheric bridge' in linking tropical Pacific ENSO events to extratropical SST anomalies. *Journal of Climate*, *9*, 2036–2057.

Mann, K. H., & Lazier, J. R. N. (1991). *Dynamics of marine ecosystems, biological-physical interactions in the oceans.* Boston: Blackwell Scientific Publications 466 pp.

Mantua, N. J., Hare, S. R., Zhang, Y., Wallace, J. M., & Francis, R. (1997). A Pacific interdecadal climate oscillation with impacts on salmon production. *Bulletin of the American Meteorological Society*, *78*, 1069–1079.

Meehl, G. A. (1990). Seasonal cycle forcing of the El Niño–Southern Oscillation in a global, coupled ocean-atmosphere GCM. *Journal of Climate*, *3*, 72–98.

McFarlane, G. A., & Beamish, R. J. (1992). Climatic influence linking copepod production with strong year-classes in sablefish, *Anoplopoma fimbria*. *Canadian Journal of Fisheries and Aquatic Sciences*, *49*, 743–753.

Meyers, S. D., Johnson, M. A., Liu, M., O'Brien, J. J., & Spiesberger, J. L. (1996). Interdecadal variability in a numerical model of the northeast Pacific Ocean: 1970–89. *Journal of Physical Oceanography*, *26*, 2635–2652.

Miller, A. J., Cayan, D. R., & White, W. B. (1998). A westward-intensified decadal change in the North Pacific thermocline and gyre-scale circulation. *Journal of Climate*, *11*, 3112–3127.

Monterey, G. I., & Levitus, S. (1997). *Climatological Cycle of Mixed Layer Depth in the World Ocean.* U.S. Gov. Printing Office, NOAA NESDIS, 5, 87 pp.

Mysak, L. A. (1986). El Niño, interannual variability and fisheries in the northeast Pacific Ocean. *Canadian Journal of Fisheries and Aquatic Sciences*, *43*, 464–497.

Nakamura, H., Lin, G., & Yamagata, T. (1997). Decadal climate variability in the North Pacific in recent decades. *Bulletin of the American Meteorological Society*, *78*, 2215–2226.

Namias, J., & Born, R. M. (1970). Temporal coherence in North Pacific sea-surface temperature patterns. *Journal of Geophysical Research*, *75*, 5952–5955.

Namias, J., & Born, R. M. (1974). Further studies of temporal coherence in North Pacific sea surface temperatures. *Journal of Geophysical Research*, *79*, 797–798.

Norris, J. R., Zhang, Y., & Wallace, J. M. (1998). Role of clouds in summertime atmosphere-ocean interactions over the North Pacific. *Journal of Climate*, *11*, 2482–2490.

Pares-Sierra, A., & O'Brien, J. J. (1989). The seasonal and interannual variability of the California Current System: a numerical model. *Journal of Geophysical Research*, *94*, 3159–3180.

Philander, S. G. (1990). *El Niño, La Niña, and the Southern Oscillation.* San Diego: Academic Press, Inc. 293 pp.

Peng, S., Mysak, L. A., Ritchie, H., Derome, J., & Douglas, B. (1995). The differences between early and midwinter responses to sea surface temperature anomalies in the northwest Atlantic. *Journal of Climate*, *8*, 137–157.

Polovina, J. J., Mitchum, G. T., & Evans, G. T. (1995). Decadal and basin-scale variation in mixed layer depth and the impact on biological production in the Central and North Pacific, 1960–88. *Deep-Sea Research I*, *42*, 1701–1716.

Polovina, J. J., Mitchum, G. T., Graham, N. E., Craig, M. P., DeMartini, E. E., & Flint, E. N. (1994). Physical and biological consequences of a climate event in the central North Pacific. *Fisheries Oceanography*, *3*, 15–21.

Reynolds, R. W., & Smith, T. M. (1994). Improved global sea surface temperature analyses using optimum interpolation. *Journal of Climate*, *7*, 929–948.

Robertson, A. W. (1996). Interdecadal variability over the North Pacific in a multi-century climate simulation. *Climate Dynamics*, *12*, 227–241.

Roemmich, D., & McGowan, J. A. (1995). Climatic warming and the decline of zooplankton in the California Current. *Science*, *267*, 1324–1326.

Sarmiento, J. L., Slater, R. D., Fasham, M. J. R., Ducklow, H. W., Togweiller, R. W., & Evans, G. T. (1993). A seasonal three-dimensional ecosystem model of nitrogen cycling in the North Atlantic euphotic zone. *Global Biogeochemical Cycles*, *7*, 415–450.

Snedecor, G. W., & Cochran, W. G. (1981). *Statistical Methods*. Seventh Addition. The Iowa State University Press, Ames, Iowa, 507 pp.

Smith, T. M., Reynolds, R. W., Livezey, R. E., & Stokes, D. C. (1996). Reconstruction of historical sea surface temperatures using empirical orthogonal functions. *Journal of Climate*, *9*, 1403–1420.

Talley, L. D. (1999). Simple coupled midlatitude climate models. *Journal of Physical Oceanography*, *29*, 2016–2037.

Tanimoto, Y., Iwasaka, N., Hanawa, K., & Toba, Y. (1993). Characteristic variations of sea surface temperature with multiple time scales in the North Pacific. *Journal of Climate*, *6*, 1153–1160.

Trenberth, K. E., & Hurrell, J. W. (1994). Decadal atmosphere-ocean variations in the Pacific. *Climate Dynamics*, *9*, 303–319.

Venrick, E. L., McGowan, J. A., Cayan, D. A., & Hayward, T. L. (1987). Climate and chlorophyll a: long-term trends in the central North Pacific Ocean. *Science*, *238*, 70–72.

Watanabe, M., & Kimoto, M. (2000). On the persistence of decadal SST anomalies in the North Atlantic. *Journal of Climate*, *13*, 3017–3028.

Weare, B. C., & Nasstrom, J. S. (1982). Examples of extended empirical orthogonal function analyses. *Monthly Weather Review*, *110*, 481–485.

Weare, B. C., Navato, A. R., & Newell, R. E. (1976). Empirical orthogonal analysis of Pacific Ocean sea surface temperatures. *Journal of Physical Oceanography*, *6*, 671–678.

White, W. B. (1995). Design of a global observing system for gyre-scale upper ocean temperature variability. *Progress in Oceanography*, *36*, 169–217.

Yukimoto, S., Endoh, M., Kitamura, Y., Kitoh, A., Motoi, T., Noda, A., & Tokioka, T. (1996). Interannual and interdecadal variabilities in the Pacific in an MRI coupled GCM. *Climate Dynamics*, *12*, 667–683.

Yoklavich, M. M., Loeb, V. J., Nishimoto, M., & Daly, B. (1996). Nearshore assemblages of larval rockfishes and their physical environment off Central California during an extended El Niño event, 1991–1993. *Fishery Bulletin*, *94*, 766–782.

Zhang, Y., Wallace, J. M., & Battisti, D. S. (1997). ENSO-like interdecadal variability. *Journal of Climate*, *10*, 1004–1020.

Zhang, Y., Norris, J. R., & Wallace, J. M. (1998). Seasonality of large-scale atmosphere-ocean interaction over the North Pacific. *Journal of Climate*, *11*, 2473–2481.